International Journal of Nanomedicine

Dovepress
open access to scientific and medical research

Open Access Full Text Article

ORIGINAL RESEARCH

Highly sensitive electron paramagnetic resonance nanoradicals for quantitative intracellular tumor oxymetric images

This article was published in the following Dove Press journal:
International Journal of Nanomedicine

Nai-Tzu Chen[1]
Eugene D Barth[2,3]
Tsung-Hsi Lee[4]
Chin-Tu Chen[5]
Boris Epel[2,3]
Howard J Halpern[2,3]
Leu-Wei Lo[5,6]

[1]Institute of New Drug Development, China Medical University, Taichung 40402, Taiwan; [2]Department of Radiation and Cellular Oncology, University of Chicago, Chicago, IL 60637, USA; [3]Center for EPR Imaging In Vivo Physiology, University of Chicago, Chicago, IL 60637, USA; [4]Department of Biological Science and Technology, China Medical University, Taichung 40402, Taiwan; [5]Department of Radiology, University of Chicago, Chicago, IL 60637 USA; [6]Institute of Biomedical Engineering and Nanomedicine, National Health Research Institutes, Zhunan 35053, Taiwan

Purpose: Tumor oxygenation is a critical parameter influencing the efficacy of cancer therapy. Low levels of oxygen in solid tumor have been recognized as an indicator of malignant progression and metastasis, as well as poor response to chemo- and radiation therapy. Being able to measure oxygenation for an individual's tumor would provide doctors with a valuable way of identifying optimal treatments for patients.

Methods: Electron paramagnetic resonance imaging (EPRI) in combination with an oxygen-measuring paramagnetic probe was performed to measure tumor oxygenation in vivo. Triarylmethyl (trityl) radical exhibits high specificity, sensitivity, and resolution for quantitative measurement of O_2 concentration. However, its in vivo applications in previous studies have been limited by the required high dosage, its short half-life, and poor intracellular permeability. To address these limitations, we developed high-capacity nanoformulated radicals that employed fluorescein isothiocyanate-labeled mesoporous silica nanoparticles (FMSNs) as trityl radical carriers. The high surface area nanostructure and easy surface modification of physiochemical properties of FMSNs enable efficient targeted delivery of highly concentrated, nonself-quenched trityl radicals, protected from environmental degradation and dilution.

Results: We successfully designed and synthesized a tumor-targeted nanoplatform as a carrier for trityl. In addition, the nanoformulated trityl does not affect oxygen-sensing capacity by a self-relaxation or broadening effect. The FMSN-trityl exhibited high sensitivity/response to oxygen in the partial oxygen pressure range from 0 to 155 mmHg. Furthermore, MSN-trityl displayed outstanding intracellular oxygen mapping in both in vitro and in vivo animal studies.

Conclusion: The highly sensitive nanoformulated trityl spin probe can profile intracellular oxygen distributions of tumor in a real-time and quantitative manner using in vivo EPRI.

Keywords: tumor oxygenation, electron paramagnetic resonance imaging (EPRI), mesoporous silica nanoparticles (MSNs), triarylmethyl (trityl) spin probe

Introduction

Tumors with lower levels of oxygen, known as hypoxia, have been recognized to increase malignant progression and metastasis, as well as respond poorly to chemo- and radiation therapy.[1–4] Several agents exist that can be administered to patients prior to radiotherapy to reduce hypoxia, such as high oxygen content gas breathing or nicotinamide, but these have not shown sufficient benefit to warrant widespread clinical use.[5] Being able to measure oxygenation for an individual's tumor would provide doctors with a valuable way of identifying the best treatment for patients. In order to understand oxygen

Correspondence: Leu-Wei Lo
Institute of Biomedical Engineering and Nanomedicine, National Health Research Institutes, No 35 Keyan Rd, Zhunan Township, Miaoli County, 35053, Taiwan
Tel +8 863 724 6166 # 37115
Fax +88 63 758 6440
Email lwlo@nhri.org.tw

submit your manuscript | www.dovepress.com
DovePress
http://doi.org/10.2147/IJN.S194779

concentration (pO_2) of tumor microenvironment, numerous studies have attempted to address this issue by utilizing oxygen-sensitive fluorescence, phosphoresce, or radioactive probes in tumors and tissues of living animals. First, oxygen electrode provides quantitative and reliable oxygen measurement and has been used as a gold standard for oxygen detection and in vivo local oxygen calibration, especially for the development of new oxygen measurement techniques.[6–8] However, invasive, point measurement approaches make it difficult for clinical use. NIR-fluorescence probes and phosphorescence lifetime measurement have also been employed to estimate partial pressures of oxygen tension in tumor.[9–11] Unfortunately, the penetration depth of optical light in living animals is limited. Optical signals also have some potential interference from biological molecules. To more closely approach clinical use, three-dimensional in vivo imaging for hypoxia has been achieved with positron emission tomography (PET), magnetic resonance imaging (MRI), and electron paramagnetic resonance imaging (EPRI). ^{18}F-misonidazole with PET has shown a strong correlation with treatment outcome in head and neck cancer[12] and tumor metastasis.[13] Tachibana et al also found ^{18}F-misonidazole to be used as a clinical prognostic indicator of radiotherapy for tumor hypoxia detection.[14] However, studies have concerns for the high background from nonmetabolized drug of ^{18}F-misonidazole.[15] ^{62}Cu-diacetyl-bis(N4-methlythiosemicarbazone (^{62}Cu-ATSM) with PET was also used to find a "hot spot" to guide intensity-modulated radiation therapy (IMRT) to enhance radiation cure of tumors containing hypoxic regions.[16,17] Larger and longer follow-up studies are needed to refine the clinical usage of imaging hypoxia in radiation delivery. Blood oxygenation level-dependent MRI (BOLD-MRI) and dynamic contrast-enhanced MRI (DCE-MRI) are both potential and clinical approaches for tumor hypoxia imaging. However, MR oxygen signals are relative and not individually quantitative. No absolute pO_2 values can be used to compare between different patients.[18–23] Electron paramagnetic resonance (EPR) spectroscopy and imaging have been extensively utilized to measure physiological parameters, such as tissue metabolic activity, redox state, and oxygen (O_2) concentration.[19,24–29] One of the major foci of EPR spectroscopic imaging has been used to map the spatial distribution of dissolved O_2 in extracellular tissue. Owing to its high specificity, freedom from confounding variation, reproducibility, sensitivity, and noninvasiveness, EPR-based measurement of O_2 concentrations offers advantages over other techniques. Most importantly, the quantitative nature of EPRI for oximetric images is repeatable, and thus successive oxygen images can be compared between pre- and post-chemo- or radiotherapy treatments, and also compared between patients. Triarylmethyl (trityl), an EPR oxygen measurement agent, exhibits high stability and narrow line width under physiological conditions. However, its in vivo applications in previous studies have been limited by the required high dosage, its short half-life, and poor intracellular permeability.[30,31] This makes intracellular pO_2 imaging impossible. To address these limitations, we developed a novel nanoformulated fluorescent mesoporous silica nanoparticle (FMSN) EPR spin probe, FMSN-trityl, to facilitate in vivo measurement of tumor oxygenation using EPRI. Here, we employed FMSNs as carriers for trityl. MSNs' unique physical properties, such as high surface areas, low systemic toxicities, and flexible functionalization of their three topological domains, make them ideal as carriers for intracellular oxygen measurement. 1) Nanochannel: the nanostructure and physiochemical properties of MSNs provided trityl radical protection from degradation inside living animal cells, to profile real-time intracellular oxygen distributions within the region of interest. 2) Framework: fluorophores were co-condensed into the silica framework of MSNs to enable fluorescence tracking both in vitro and in vivo. 3) Exterior surface: FMSN exteriors were labeled with polyethylene glycol (PEG) polymers to increase their water solubility, and labeled with tumor-associated glycoprotein 72 (TAG-72), a glycoprotein found on the surface of many cancer cells as a targeting moiety. To the best of our knowledge, this is the first study to use a nanoformulated spin probe for quantitative intracellular tumor oximetric images.

Materials and methods

Materials

The materials employed in this study are listed as follows: ammonium hydroxide (NH_4OH, 30–33%, Sigma-Aldrich, Darmstad, Germany), hexadecyltrimethylammonium bromide (CTAB, 99%, Alfa Aesar, Haverhill, MA, USA), tetraethoxysilane (TEOS, 98%, Sigma-Aldrich), ammonium nitrate (NH_4NO_3, Sigma-Aldrich), 3-aminopropyltriethoxysilane (APTES, 99%, Sigma-Aldrich), N-trimethoxysilylpropyl-N,N,N-trimethylammonium chloride (TA), N-octane (Alfa Aesar), ethanol (99.5%, J.B. Baker, Phillipsburg, NJ, USA), fluorescein isothiocyanate (FITC, Thermo Fisher Scientific, Waltham, MA, USA), silane PEG-NHS (PG2-NSSL-1k, Nanocs, New York, NY, USA), TAG72mAb (CC49, GTX17361, GeneTex, Irvine, CA, USA), wheat germ

agglutinate AlexaFluor 594 (WGA-594, Thermo Fisher Scientific), PBS (Thermo Fisher Scientific), ProLong® Diamond Antifade Mountant (Thermo Fisher Scientific), Hoechst 33,342 (AAT Bioquest, Sunnyvale, CA, USA), tiarylmethyl (OX063d24 trityl(methyl-tris[8-carboxy-2,2,6,6-tetrakis[(2-hydroxy-2d_2-ethyl]benzo[1,2-d:4,5-d0] bis[1,3] dithiol-4-yl], trisodium salt (GE Healthcare, London, UK), and vinyl polysiloxane mode material (GC America Inc., Alsip, IL, USA).

Preparation of nanoparticles

Synthesis of FMSNs and modification of PEG and TAG72mAb

FMSNs were synthesized according to our previous studies.[32,33] 1 mg of FITC was stirred in an APTMS–ethanol solution (0.1 M in 5 mL of ethanol) in complete darkness for 24 hrs to synthesize FITC-APTMS. 0.58 g of cetyltrimethylammonium bromide (CTAB) was completely dissolved in 300 mL of 0.17 M ammonium hydroxide (NH_4OH), and 5.0 g of n-octane was added into the mixed solution for pore size enlargement. After stirring gently at 40°C for 1 hr, 5 mL of FITC-APTMS and 5 mL of 0.2 M TEOS were introduced into the mixed solution. 4 hrs later, 1.0 M TEOS was added dropwise into the mixed solution. The solution was then stirred for another 1 hr, followed by aging for 24 hrs at 40°C. As-synthesized FMSNs were then collected and washed by centrifugation (12,000 rpm for 30 mins) three times and subsequently dispersed in 99.5% ethanol. To increase water solubility, PEG was utilized to modify the surfaces of FMSNs. 75 mg FMSN was resuspended in ethanol and stirred with 25 mg of silane-PEG-NHS at 60°C for 24 hrs. For CTAB template removal, the as-synthesized FMSNs were refluxed with 250 mg ammonium nitrate in 99.5% ethanol at 60°C for 2 hrs. Then, N-trimethoxysilylpropyl-N, N,N-trimethylammonium chloride (TA) silanes were used to increase the positive charge of nanoparticle. 300 µL of TA was mixed with extracted FMSN products described above at 60°C overnight and followed by EtOH washing three times. The collected FMSN products were washed and reacted with 200 µL of TAG72mAb in PBS for 2 hrs at 4°C. The final products were then collected by 12,000 rpm centrifuging and redispersed in water.

Loading of FMSN-PEG-TAG72 with trityl

Triarylmethyl (trityl) spin probe, OX063d24 trisodium salt, was first dissolved in water, and the pH was adjusted to 7.4. 384 µL of 12.4 mM OX063d24 trityl was mixed with 20 mg FMSN-PEG-TAG72 for 2 hrs at room temperature. The loaded products were then collected and washed by 12,000 rpm centrifuging. The dark green color of OX063d24 trityl was dissolved in the aqueous solution well prior to the reaction. After 2 hrs of reaction and centrifuging, the supernatant appeared light green, and the pellets (FMSNs with trityl) exhibited a dark green color. The quantitative loading capacity was evaluated from the 468 nm absorption of trityl by UV-Vis spectrophotometer (Agilent, Santa Clara, CA, USA).

Oxygen response and cell oxygen consumption

The oxygen-sensing triarylmethyl (trityl) EPR spin probe used in this study is OX063d24, deuterated OX063, and has a peak-to-peak line width of 8 mG, which is half that of native isotope abundance (OX063, 16 mG).[34–36] 0%, 3%, 6%, 9%, and 21% of oxygen were bubbled in a sealed vial containing either trityl (OX063d24) or FMSN-trityl (FMSN with OX063d24) samples for 20 mins until equilibrium. EPR scanning was then performed. The EPR spectra were recorded at room temperature using 250 MHz EPR spectroscopy (Center of EPR Imaging In Vivo Physiology, The University of Chicago) with the following parameters: modulation frequency of 5 kHz, time constant of 1 ms, power of 5.00 mW, scan points of 512, dwell time of 1 ms, and scan field width of 2.5 G. For cell oxygen consumption assay, FMSN-trityl treated cells were washed and collected into a sealed quartz flat cell chamber. The loading/processing time was controlled within 5 mins before the EPR scan to obtain the most accurate oxygen information. The following parameters were used for the Bruker X-band EPR spectrometer: frequency of 9.42 GHz, microwave power of 2 mW, modulation frequency of 100 kHz, scan points of 512, dwell time of 1 ms, and modulation amplitude of 0.06 G.

In vitro cell uptake and competition assay

Human colon adenocarcinoma LS-174T cells were obtained from the American Type Culture Collection (Rockville, MD, USA). LS-174T cells expressed TAG-72 glycoprotein and were used as a positive control to evaluate the binding efficiency for TAG-72 monoclonal antibody or binding peptide.[37,38] LS-174T cells were treated with PBS (control), trityl-loaded FMSN-PEG or trityl-loaded FMSN-PEG-TAG72 for 2 hrs, and the cells were washed by PBS three times. Confocal imaging (Leica TCS SP5, Wetzlar, Germany) and flow cytometry (BD Facscanto, Piscataway, NJ, USA) were then performed.

Ethics statement

Animals used in these studies were approved under the guidelines of the Institutional Animal Care and Use Committee (IACUC) of the University of Chicago, which complies with the guidelines outlined by the National Institutes of Health. The authorization number for Animal Use and Care Procedure (ACUP) is 71,697.

Tumor preparation and location

Six-week-old male nude mice were subcutaneously inoculated with 2 million LS-174T cells in the middle distal hind legs. Tumor was grown to 250 mm^3 prior to EPR imaging. Gas anesthesia with 1–2% isofluorane mixed with medical grade air was adjusted to regularize breathing and prevent animal motion during the injection and imaging. Respiration frequency and depth were monitored continuously. The tumor was immobilized with soft elastic vinyl polysiloxane dental mold material. A digital needle probe thermometer was used to measure rectal temperature. The temperature was maintained at 36°C to 37°C with heating lamps. MRI location of the tumor was obtained with a rapid acquisition with refocused echoes (RARE). Spin-echo images were acquired at 9.4 T on an Omega Bruker/GE imager with the following parameters: repetition time=3,000 ms, effective excitation time=56 ms, field of view=3.0 cm, matrix size=256×256, slice thickness=1 mm, NEX=1, and rare factor=8. The MRI with the water fiducials was registered with an image of the EPR fiducials, according to previous studies.[35,39]

In vivo EPR imaging

An MRI as noted above defined the 3D tumor boundary, EPR images of extracellular pO_2 were acquired with spin-lattice relaxation oxygen imaging[40] in 10 mins using a 250 MHz pulse EPR imager.[41,42] p pO_2 image was initially acquired with bolus intravenous (IV) injection of 135 μL of80 mM OX063d24 spin probe (0.43 mmols/kg) solution and followed by 3.5 μL/min continuously infusion over 30 mins during three pO_2 images. OX063d24 is a partially deuterated trisodium salt of methyl-tris[8-carboxy-2,2,6,6-tetrakis[2-hydroxy-12H-ethyl]benzo [1,2-d:4,5-d']bis [1,3]dithiol-4-yl]-trisodium salt (MW 1451). It was synthesized by the Novosibirsk Institute of Organic Chemistry.[43] It is available as OX71 from GE Healthcare (Little Chalfont, Buckinghamshire, UK). One-half hour after the IV infusion, 3.36 mg FMSN-trityl-loaded nanostructures containing 0.21 mg trityl was injected intratumorally covering the tumor at six equally spaced superficial locations and two deep locations to produce a uniform distribution.[44]

Results and discussion

In this study, we developed a novel trityl-loaded FMSN to facilitate in vivo measurement of tumor oxygenation using EPR oximetry. We employed FMSNs as a carrier for triarylmethyl (trityl), an EPR oxygen detection agent, for intracellular oxygenation measurement (Figure 1). Figure 1A illustrates the scheme of trityl-loaded FMSNs for EPR imaging. PEG was modified on the exterior surface of FMSNs to increase the water solubility in physiological environment. TAG72mAb, the tumor-targeting moiety, was applied to the surface of FITC-labeled MSN as a carrier for trityl radical for in vivo tumor oxygen measurement. The positive charge from TA of FMSNs interacts with trityl radical by electrostatic interaction. The loading capacity of FMSN-PEG-TAG72 for trityl radical was detected by 468 nm absorption of trityl through UV-Vis spectrophotometer; it was found to reach 6.14%. Figure 1B shows transmission electron microscope (TEM) image of FMSNs with average size of approximately 70 nm in diameter. Conjugation of PEG/TAG72mAb to FMSNs, confirmed by thermogravimetric analysis, demonstrated weight losses of FMSN, FMSN-PEG, and FMSN-PEG-TAG72 of 10.1%, 20.2%, and 22.1%, respectively, as shown in Figure 1C. Figure 1D shows the EPR spectra of trityl radial and FMSN-trityl under an argon gas (0% oxygen) environment. Trityl radical (Figure 1D, black line) presents a unique sharp shape spectrum, and the peak-to-peak line width is approximately 80 mG. The spectrum of trityl radical encapsulated in FMSNs (FMSN-trityl, Figure 1D, red line) remained in the same shape and sharp peak as trityl alone, which implied that the electrostatic interaction between the TA group of FMSNs and the carboxylic acid of trityl does not affect the oxygen-sensing capacity of the spin probe by a self-relaxation or broadening effect.

In order to demonstrate the oxygen-sensing ability of FMSN-trityl, we bubbled argon gas (0% oxygen), 3, 6, 9% oxygen-containing gas, or medical grade air (21% oxygen) into vials with FMSN-trityl/trityl-only aqueous solution and monitored the EPR spectrum. Both trityl and FMSN-trityl exhibited a high sensitivity/response to oxygen in the pO_2 range from 0 to 155 mmHg (0~21% oxygen) (Figure 2A). The peak-to-peak line width of the spectra was plotted with oxygen concentration and pO_2 (mmHg), as shown in Figure 2B. Directly proportional graphs were found for both trityl and FMSN-trityl, and this result strongly suggested that FMSN-trityl can not only be used as a spin probe for oxygen sensing, but also maintain high

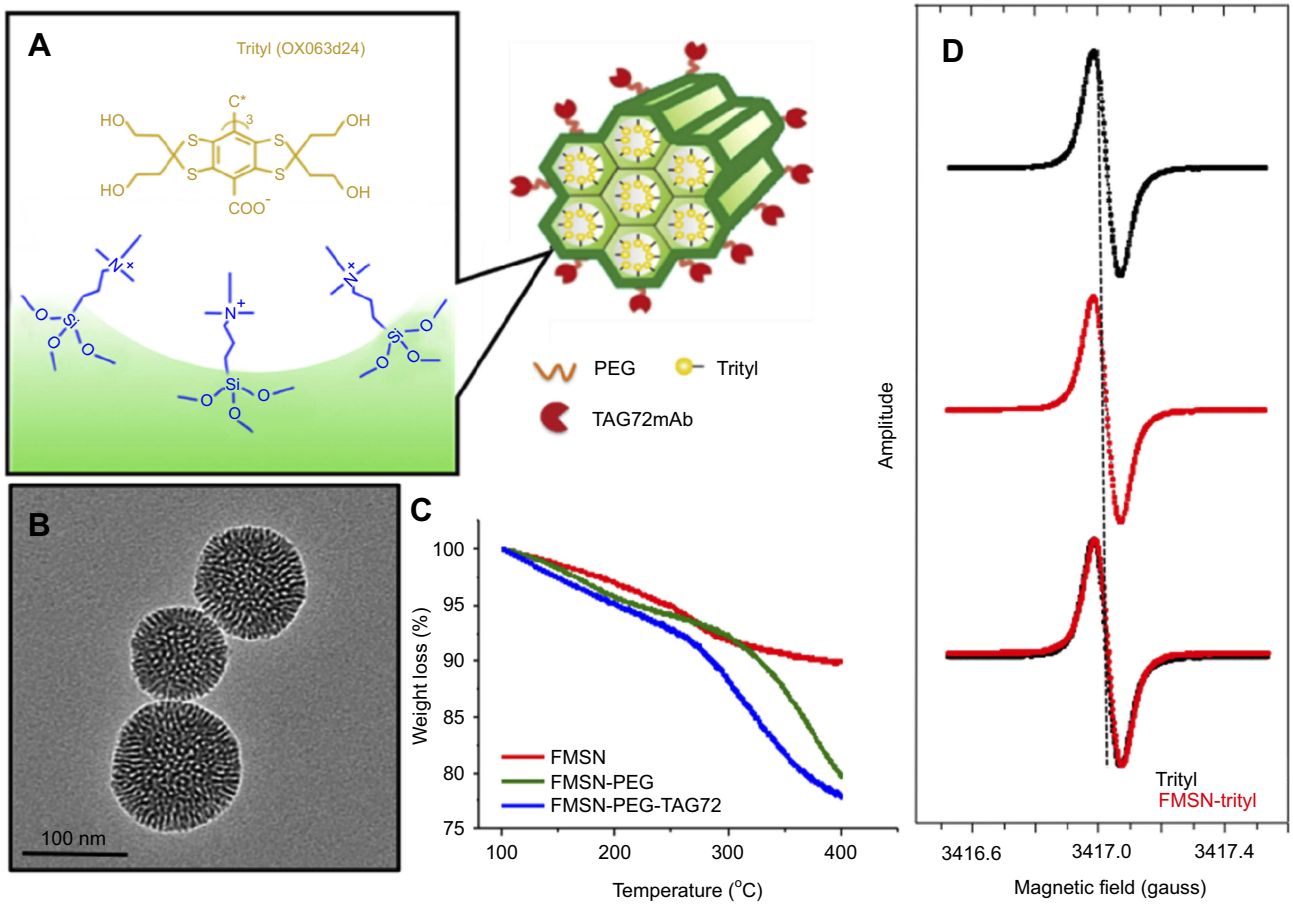

Figure 1 (**A**) Illustration of trityl-loaded FMSNs for electron paramagnetic resonance imaging. FMSN with targeting moiety, TAG72mAb, as a carrier for trityl radical for in vivo tumor oxygen measurement. (**B**) Transmission electron microscope (TEM) image of mesoporous silica nanoparticles. (**C**) Thermogravimetric analysis of FMSN, FMSN-PEG, and FMSN-PEG-TAG72. (**D**) EPR spectrum of trityl (black), FMSN-trityl (red), and overlay.

sensitivity as trityl alone. Trityl encapsulated in FMSNs provided a reversible oxygen sensing (data not shown) that was able to report dynamic real time in situ oxygen mapping. The nanosystem possessed great physical properties that can target specific tumors, report intracellular oxygen information, and extend imaging time. Furthermore, we clarified the possible effect of pH levels on oxygen sensing for the trityl spin probe. FMSN-trityl aqueous solutions were adjusted to indicate pH (3, 5, 7, 9, 11), bubbled with air, and the spectrum and peak-to-peak line width were acquired. The measurements from FMSN-trityl were found to be consistent with the previous data, and no impact was observed by changing the pH of the aqueous solution (Figure 2C). This is extremely important for our study, especially for cell study and in vivo animal demonstration, since pH levels in cells or tumor areas may exhibit marked changes, such as endosome or lysosome, and acidic environment of tumor.[45,46]

Figure 3 illustrates the localization and cell uptake efficacy of FMSN-trityl by using confocal microscopy and flow cytometer. LS-174T cells were treated with PBS (Figure 3A), trityl-loaded FMSN-PEG (Figure 3B), or trityl-loaded FMSN-PEG-TAG72 (Figure 3C) for 2 hrs and extracellular particles were washed out by PBS. The cells were also counterstained with nucleus (blue) and cell membrane (red) staining agents. In Figure 3C, confocal image showed that the fluorescence-labeled MSNs were uptaken by cells and localized in the cytoplasm. We further quantified the cell uptake levels of TAG72mAb-labeled FMSNs. 55% cellular uptake efficacy was found, which constitutes 3.5 times enhancement of cell uptake compared with nontargeted FMSN-PEG (Figure 3D). Cells treated with PBS were served as control. The results from Figure 3 provide evidence that FMSN-trityl has the ability to penetrate the cell membrane and obtain intracellular oxygen information.

In an attempt to demonstrate oxygen sensing in a more complicated system, we performed a cell oxygen consumption assay. Five million cells were treated with the targeted FMSN-trityl for 2 hrs, and the extracellular nanoparticles

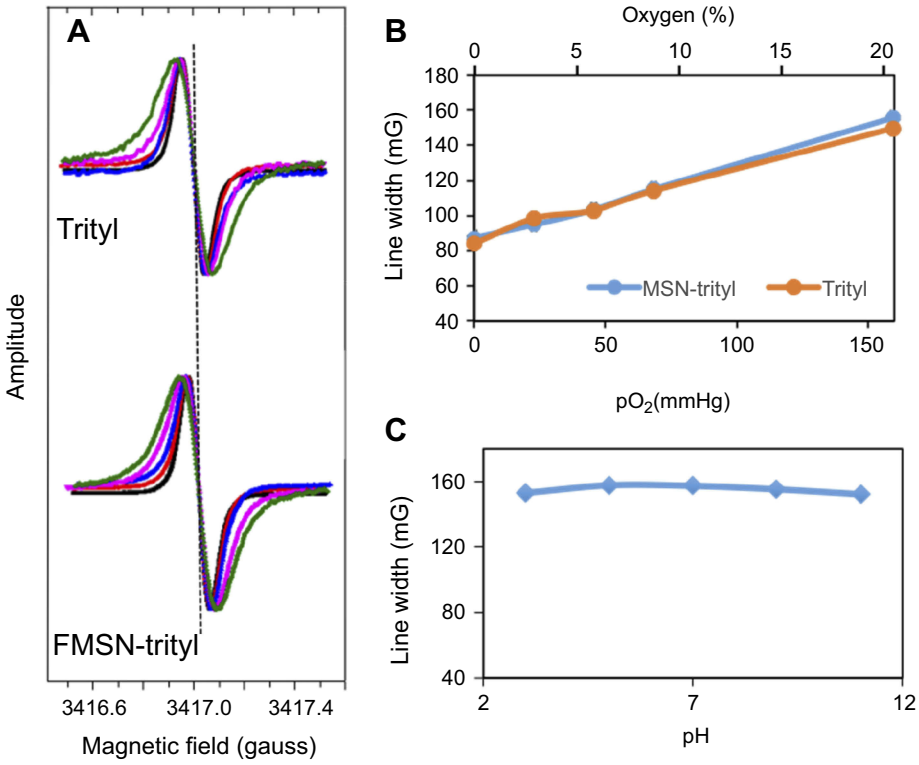

Figure 2 Oxygen response of FMSN-trityl. (**A**) EPR spectrum of trityl and FMSN-trityl at various oxygen concentrations. The spectra are scaled to the same maximum amplitude height in the plots. (**B**) The dependence of peak-to-peak EPR spectrum line width of trityl/FMSN-trityl on oxygen partial pressure. (**C**) The dependence of peak-to-peak EPR spectrum line width of FMSN-trityl at different pH levels.

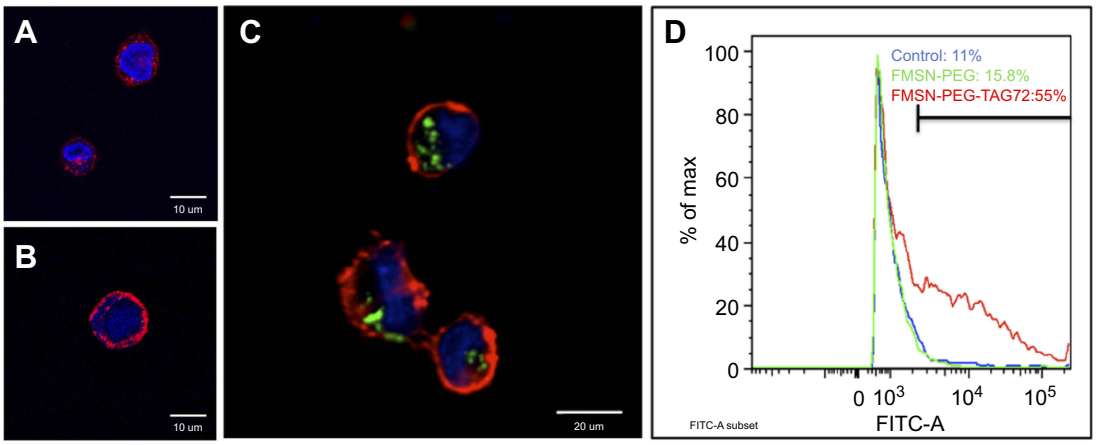

Figure 3 Cell uptake of FMSN-trityl. Fluorescent confocal images of cells treated with (**A**) PBS, (**B**) trityl-loaded FMSN-PEG, (**C**) trityl-loaded FMSN-PEG-TAG72. Trityl-loaded FITC-MSNs (green); nucleus stain, DAPI (blue); and cell membrane stain, WGA647 (red). (**D**) Histogram of cell counts from flow cytometer. *X*-axis shows the intensity of FITC.

were washed out by PBS three times. Treated cells were then trypsinized and loaded into a quartz-sealed flat chamber. EPR spectra were constantly scanned in a function of time for 900 s. Figure 4 shows the kinetics of oxygen consumption measured by EPR in a suspension of LS-174T cells. Several spectra from representative time points are shown in Figure 4A, and measured partial oxygen pressure with time is plotted in Figure 4B. The starting pO_2 was approximately 130 mmHg, which was consistent with another study,[47] which showed that 8–9 mg/L dissolved oxygen at room temperate water and pO_2 continued to decrease at a rate of 0.075 mmHg/s. Oxygen partial pressure became flatter after 900 s, which might be ascribed to the ambient temperature-induced apoptosis or low metabolism of cells. However, the

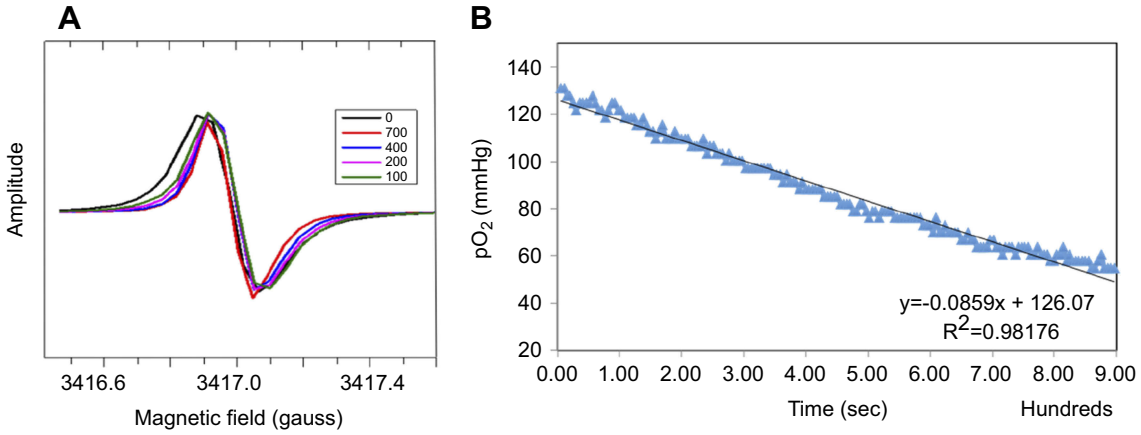

Figure 4 Cell oxygen consumption. (**A**) EPR spectra of cells treated with trityl-loaded FMSN-PEG-TAG72 at various time points. (**B**) The peak-to-peak line width of EPR spectra was converted to pO_2 (mmHg) and plotted with time. Dwell time per scan is 5.12 s.

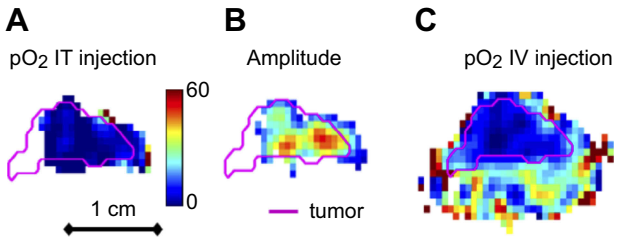

Figure 5 In vivo tumor oxygen images. Nude mice with LS-174T xenograft tumor on leg flank were used to monitor in vivo oxygen measurements. pO_2 of tumor was first imaged by intravenously injected trityl. After half-hour washout, tumor mice were injected with 3.36 mg of FMSN-trityl and the intracellular pO_2 levels were monitored by EPRI. Tumor outlines obtained from MRI were illustrated in pink. Color bar showed pO_2 scale in the range 0–60 mmHg. (**A**) pO_2 image measured from FMSN-trityl via IT injection. (**B**) Signal amplitude acquired from FMSN-trityl via IT injection. (**C**) pO_2 image measured from trityl via IV injection.

significant decline of oxygen concentration showed the sensitive oxygen response of FMSN-trityl within a relatively complicated cell system.

For in vivo tumor oxygenation, we used xenograft tumor mice for tumor oxygen EPRI study. The leg/tumor was immobilized with soft elastic vinyl polysiloxane dental mold material. pO_2 distributions of tumor were first imaged by intravenously injected bolus of trityl spin probe and followed by 3.5 μL/min continuous infusion over 30 mins during three pO_2 images. After half-hour washout, tumor mice were than intratumorally injected with 3.36 mg trityl-loaded FMSNs and monitored by EPRI for 1 hr. Three 1 mm inner diameter, 3 to 4 cm long borosilicate glass sample tubes containing either 10 mmol/L trityl (EPR imaging) or water (MRI) were placed at various angles as fiducial markers for co-registration of EPR imaging with MRI. With MRI for image registration and anatomical guidance, the tumor outline could be contoured and transferred to an EPR image (pink outline in Figure 5). Figure 5A displays the pO_2 distribution measured from FMSN-trityl. Amplitude image from Figure 5B shows the concentration of FMSN-trityl EPR signal. Figure 5C shows the pO_2 mapping measured from trityl. In vivo results revealed an outstanding oxygen response of the hypoxia tumor area, from 5.8 to 12.4 torr of pO_2 (data not shown). Low oxygen distribution was found on the left side of the tumor. The result suggested that the FMSN-trityl performed high oxygen sensitivity in a wide oxygen range, especially within the low oxygen hypoxia region.

Conclusions

The design of a nanoformulated EPR spin probe was intended to demonstrate the feasibility of using mesoporous silica nanoparticle as a carrier for tumor oxygen mapping. Nanoformulated trityl not only exhibited a narrow sharp spectrum, but also demonstrated high sensitivity and positive correlation to oxygen concentration. The in vitro and in vivo animal study achieved excellent performance in pO_2 images. Overall, the results from this study indicated that FMSN-trityl demonstrated the first quantitative intracellular oxygen mapping using EPR; and the low dosage and long imaging window further augmented the value of this FMSN-trityl oxygen probe compared to others. We believe that FMSN-trityl provides high-value tumor oxygen information for in situ diagnostic imaging for potential clinical uses.

Acknowledgments

This research was funded by BN-106-PP-04 (National Health Research Institutes, Taiwan), NSC100-2911-I-400-502, MOST 106-2113-M-039-002-MY2, MOST 107-

2113-M-039-003-MY2 (Ministry of Science and Technology of Taiwan), CMU107-N-20 (China Medical University), PDR-075 (Chicago Biomedical Consortium), USA NIH P41 EB002034 and R01 CA098575.

Disclosure

Prof. Dr. Leu-Wei Lo reports grants from National Health Research Institutes, Taiwan and the Ministry of Science and Technology of Taiwan. Dr. Nai-Tzu Chen reports grants from China Medical University, Taiwan, Chicago Biomedical Consortium, and the Ministry of Science and Technology of Taiwan. Prof. Dr. Howard J Halpern reports grants from USA NIH, during the conduct of the study and has patents 8,664,955, 9,392,957, 4,714,886, and 5,431,901 issued. The other authors report no conflicts of interest in this work.

References

1. Rockwell S, Dobrucki IT, Kim EY, Marrison ST, Vu VT. Hypoxia and radiation therapy: past history, ongoing research, and future promise. *Curr Mol Med*. 2009;9(4):442–458.
2. Horsman MR, Mortensen LS, Petersen JB, Busk M, Overgaard J. Imaging hypoxia to improve radiotherapy outcome. *Nat Rev Clin Oncol*. 2012;9(12):674–687. doi:10.1038/nrclinonc.2012.171
3. Guo Y, Wu M, Zhao J, Li Y. [Advances in hypoxia microenvironment and chemotherapy-resistant of lung cancer]. *Zhongguo Fei Ai Za Zhi=Chin J Lung Cancer*. 2014;17(3):265–268. doi:10.3779/j.issn.1009-3419.2014.03.14
4. Tang YA, Chen YF, Bao Y, et al. Hypoxic tumor microenvironment activates GLI2 via HIF-1alpha and TGF-beta2 to promote chemoresistance in colorectal cancer. *Proc Natl Acad Sci U S A*. 2018;115(26):E5990–E5999. doi:10.1073/pnas.1801348115
5. Overgaard J. Hypoxic radiosensitization: adored and ignored. *J Clin Oncol*. 2007;25(26):4066–4067. doi:10.1200/JCO.2007.12.7878
6. Elas M, Ahn KH, Parasca A, et al. Electron paramagnetic resonance oxygen images correlate spatially and quantitatively with Oxylite oxygen measurements. *Clin Cancer Res*. 2006;12(14 Pt 1):4209–4217. doi:10.1158/1078-0432.CCR-05-0446
7. Tran LB, Bol A, Labar D, et al. Hypoxia imaging with the nitroimidazole 18F-FAZA PET tracer: a comparison with OxyLite, EPR oximetry and 19F-MRI relaxometry. *Radiother Oncol*. 2012;105(1):29–35. doi:10.1016/j.radonc.2012.04.011
8. Ortiz-Prado E, Natah S, Srinivasan S, Dunn JF. A method for measuring brain partial pressure of oxygen in unanesthetized unrestrained subjects: the effect of acute and chronic hypoxia on brain tissue PO (2). *J Neurosci Methods*. 2010;193(2):217–225. doi:10.1016/j.jneumeth.2010.08.019
9. Zheng X, Wang X, Mao H, Wu W, Liu B, Jiang X. Hypoxia-specific ultrasensitive detection of tumours and cancer cells in vivo. *Nat Commun*. 2015;6:5834. doi:10.1038/ncomms6834
10. Hirakawa Y, Yoshihara T, Kamiya M, et al. Quantitating intracellular oxygen tension in vivo by phosphorescence lifetime measurement. *Sci Rep*. 2015;5:17838. doi:10.1038/srep17838
11. Lo LW, Koch CJ, Wilson DF. Calibration of oxygen-dependent quenching of the phosphorescence of Pd-meso-tetra (4-carboxyphenyl) porphine: a phosphor with general application for measuring oxygen concentration in biological systems. *Anal Biochem*. 1996;236:153–160. doi:10.1006/abio.1996.0144
12. Eschmann SM, Paulsen F, Reimold M, et al. Prognostic impact of hypoxia imaging with 18F-misonidazole PET in non-small cell lung cancer and head and neck cancer before radiotherapy. *J Nucl Med*. 2005;46(2):253–260.
13. McGowan DR, Macpherson RE, Bradley KM, Fenwick JD, Gleeson FV, Higgins GS. 18F-Misonidazole PET-CT scan detection of occult bone metastasis. *Thorax*. 2016;71(1):97. doi:10.1136/thoraxjnl-2015-207140
14. Tachibana I, Nishimura Y, Hanaoka K, et al. Tumor Hypoxia Detected by (18)F-fluoromisonidazole Positron Emission Tomography (FMISO PET) as a Prognostic Indicator of Radiotherapy (RT). *Anticancer Res*. 2018;38(3):1775–1781. doi:10.21873/anticanres.12415
15. Adelstein DJ. *Squamous Cell Head and Neck Cancer: Recent Clinical Progress and Prospects for the Future*. 2005th ed. Totowa, NJ: Humana Press; 2005:978–1588294739. ISBN-13
16. Vavere AL, Lewis JS. Cu-ATSM: a radiopharmaceutical for the PET imaging of hypoxia. *Dalton Trans*. 2007;(43):4893–4902.
17. Lapi SE, Lewis JS, Dehdashti F. Evaluation of hypoxia with copper-labeled diacetyl-bis(N-methylthiosemicarbazone). *Semin Nucl Med*. 2015;45(2):177–185. doi:10.1053/j.semnuclmed.2014.10.003
18. Jiang L, Weatherall PT, McColl RW, Tripathy D, Mason RP. Blood oxygenation level-dependent (BOLD) contrast magnetic resonance imaging (MRI) for prediction of breast cancer chemotherapy response: a pilot study. *J Magn Reson Imaging*. 2013;37(5):1083–1092. doi:10.1002/jmri.23891
19. Williams BB, Al Hallaq H, Chandramouli GV, et al. Imaging spin probe distribution in the tumor of a living mouse with 250 MHz EPR: correlation with BOLD MRI. *Magn Reson Med*. 2002;47(4):634–638. doi:10.1002/(ISSN)1522-2594
20. Neugarten J, Golestaneh L. Blood oxygenation level-dependent MRI for assessment of renal oxygenation. *Int J Nephrol Renovasc Dis*. 2014;7:421–435. doi:10.2147/IJNRD.S42924
21. Halle C, Andersen E, Lando M, et al. Hypoxia-induced gene expression in chemoradioresistant cervical cancer revealed by dynamic contrast-enhanced MRI. *Cancer Res*. 2012;72(20):5285–5295. doi:10.1158/0008-5472.CAN-12-1085
22. Egeland TA, Gulliksrud K, Gaustad JV, Mathiesen B, Rofstad EK. Dynamic contrast-enhanced-MRI of tumor hypoxia. *Magn Reson Med*. 2012;67(2):519–530. doi:10.1002/mrm.23014
23. Jensen RL, Mumert ML, Gillespie DL, Kinney AY, Schabel MC, Salzman KL. Preoperative dynamic contrast-enhanced MRI correlates with molecular markers of hypoxia and vascularity in specific areas of intratumoral microenvironment and is predictive of patient outcome. *Neuro-Oncology*. 2014;16(2):280–291. doi:10.1093/neuonc/not148
24. Krishna MC, Devasahayam N, Cook JA, Subramanian S, Kuppusamy P, Mitchell JB. Electron paramagnetic resonance for small animal imaging applications. *ILAR J Nat Res Counc Inst Lab Anim Resour*. 2001;42(3):209–218. doi:10.1093/ilar.42.3.209
25. Tsai P, Porasuphatana S, Halpern HJ, Barth ED, Rosen GM. In vivo in situ detection of nitric oxide using low-frequency EPR spectroscopy. *Methods Mol Biol*. 2002;196:227–237. doi:10.1385/1-59259-274-0:227
26. Reddy TJ, Iwama T, Halpern HJ, Rawal VH. General synthesis of persistent trityl radicals for EPR imaging of biological systems. *J Org Chem*. 2002;67(14):4635–4639.
27. Liu Y, Villamena FA, Sun J, Wang TY, Zweier JL. Esterified trityl radicals as intracellular oxygen probes. *Free Radic Biol Med*. 2009;46(7):876–883. doi:10.1016/j.freeradbiomed.2008.12.011
28. Driesschaert B, Marchand V, Leveque P, Gallez B, Marchand-Brynaert J. A phosphonated triarylmethyl radical as a probe for measurement of pH by EPR. *Chem commun*. 2012;48(34):4049–4051. doi:10.1039/c2cc00025c
29. Redler G, Epel B, Halpern HJ. EPR image based oxygen movies for transient hypoxia. *Adv Exp Med Biol*. 2014;812:127–133. doi:10.1007/978-1-4939-0620-8_17

30. Matsumoto K, English S, Yoo J, et al. Pharmacokinetics of a triarylmethyl-type paramagnetic spin probe used in EPR oximetry. *Magn Reson Med*. 2004;52(4):885–892. doi:10.1002/(ISSN)1522-2594
31. Matsumoto KI, Hyodo F, Mitchell JB, Krishna MC. Effect of body temperature on the pharmacokinetics of a triarylmethyl-type paramagnetic contrast agent used in EPR oximetry. *Magn Reson Med*. 2018;79(2):1212–1218. doi:10.1002/mrm.27008
32. Cheng S-H, Hsieh -C-C, Chen N-T, et al. Well-defined mesoporous nanostructure modulates three-dimensional interface energy transfer for two-photon activated photodynamic therapy. *Nano Today*. 2011;6(6):552–563. doi:10.1016/j.nantod.2011.10.003
33. Chen NT, Souris JS, Cheng SH, et al. Lectin-functionalized mesoporous silica nanoparticles for endoscopic detection of premalignant colonic lesions. *Nanomedicine*. 2017;13(6):1941–1952. doi:10.1016/j.nano.2017.03.014
34. Elas M, Magwood JM, Butler B, et al. EPR oxygen images predict tumor control by a 50% tumor control radiation dose. *Cancer Res*. 2013;73(17):5328–5335. doi:10.1158/0008-5472.CAN-13-0069
35. Elas M, Hleihel D, Barth ED, et al. Where it's at really matters: in situ in vivo vascular endothelial growth factor spatially correlates with electron paramagnetic resonance pO2 images in tumors of living mice. *Mol Imaging Biol*. 2011;13(6):1107–1113. doi:10.1007/s11307-010-0436-4
36. Elas M, Ichikawa K, Halpern HJ. Oxidative stress imaging in live animals with techniques based on electron paramagnetic resonance. *Radiat Res*. 2012;177(4):514–523.
37. Chen L, Wang Y, Cheng D, et al. Comparing two TAG-72 binding peptides previously identified by phage display as potential imaging agents. *Nucl Med Commun*. 2011;32(10):920–924. doi:10.1097/MNM.0b013e328348fc64
38. Knight JC, Mosley M, Uyeda HT, et al. In vivo pretargeted imaging of HER2 and TAG-72 expression using the halotag enzyme. *Mol Pharm*. 2017;14(7):2307–2313. doi:10.1021/acs.molpharmaceut.7b00172
39. Elas M, Magwood JM, Butler B, et al. EPR oxygen images predict tumor control by a 50% tumor control radiation dose. *Cancer Res*. 2013;73(17):5328–5335. doi:10.1158/0008-5472.CAN-13-0069
40. Epel B, Bowman MK, Mailer C, Halpern HJ. Absolute oxygen R-1e imaging in vivo with pulse electron paramagnetic resonance. *Magn Reson Med*. 2014;72(2):362–368. doi:10.1002/mrm.24926
41. Epel B, Sundramoorthy SV, Mailer C, Halpern HJ. A versatile high speed 250-MHz pulse imager for biomedical applications. *Concept Magn Reson B*. 2008;33B(3):163–176. doi:10.1002/cmr.b.20119
42. Froncisz W, Hyde JS. The loop-gap resonator: a new microwave lumped circuit ESR sample structure. *J Magn Reson*. 1982;47:515–521.
43. Kuzhelev AA, Trukhin DV, Krumkacheva OA, et al. Room-temperature electron spin relaxation of triarylmethyl radicals at the X- and Q-bands. *J Phys Chem B*. 2015;119(43):13630–13640. doi:10.1021/acs.jpcb.5b03027
44. Lammers T, Peschke P, Kühnlein R, et al. Effect of intratumoral injection on the biodistribution and the therapeutic potential of HPMA copolymer-based drug delivery systems. *Neoplasia*. 2006;8(10):788–795.
45. Huber V, Camisaschi C, Berzi A, et al., Cancer acidity: an ultimate frontier of tumor immune escape and a novel target of immunomodulation. *Seminars in Cancer Biology*, 2017, 43, 74–89. doi:10.1016/j.semcancer.2017.03.001
46. Peppicelli S, Andreucci E, Ruzzolini J, et al. The acidic microenvironment as a possible niche of dormant tumor cells. *Cell Mol Life Sci*. 2017;74(15):2761–2771. doi:10.1007/s00018-017-2496-y
47. Yu Y, Kwon MS, Jung J, et al. Room-temperature-phosphorescence-based dissolved oxygen detection by core-shell polymer nanoparticles containing metal-free organic phosphors. *Angewandte Chemie*. 2017;56(51):16207–16211. doi:10.1002/anie.201708606